

# Levels, Chemical Compositions, and Sources of PM<sub>2.5</sub> of Rural and Urban Area under the Impact of Wheat Harvest

Zhiyong Li<sup>1,2\*</sup>, Ziyuan Yue<sup>1</sup>, Dingyuan Yang<sup>1</sup>, Lei Wang<sup>3</sup>, Xin Wang<sup>3\*</sup>, Zhenxin Li<sup>1</sup>, Yutong Wang<sup>1</sup>, Lan Chen<sup>1,2</sup>, Songtao Guo<sup>1</sup>, Jinsong Yao<sup>1</sup>, Xiao Lou<sup>1</sup>, Xiaolin Xu<sup>1</sup>, Jinye Wei<sup>1</sup>

<sup>1</sup>A Hebei Key Lab of Power Plant Flue Gas Multi-Pollutants Control, Department of Environmental Science and Engineering, North China Electric Power University, Baoding 071003, China

<sup>2</sup>MOE Key Laboratory of Resources and Environmental Systems Optimization, Ministry of Education, Beijing 102206, China

<sup>3</sup>Hebei Research Center for Geoanalysis, Baoding 071003, China

## ABSTRACT

Wheat harvesting significantly alters the characteristics of PM<sub>2.5</sub> in both rural regions and the adjacent urban areas. We conducted a systematic PM<sub>2.5</sub> sampling campaign at two sites, one rural (ARS) and the other urban (UA), in the center of the Beijing-Tianjin-Hebei megalopolis during and after the wheat harvest (WH). The PM<sub>2.5</sub> concentrations at ARS and UA decreased from 156 to 75.5  $\mu\text{g m}^{-3}$  and from 137 to 53.1  $\mu\text{g m}^{-3}$ , respectively, between the periods during (DWH) and after (AWH) the wheat harvest. The hysteresis of the PM<sub>2.5</sub> peaks at UA confirmed the rural-to-urban migration of pollution. Additionally, we found high geo-accumulation index ( $I_{\text{geo}}$ ) values for crustal elements at both sampling sites, indicating that the dust emissions originated from the WH. Between DWH and AWH, the share of soil dust in the PM<sub>2.5</sub> decreased from 21.3% to 7.98% and from 9.40% to 6.75% at ARS and UA, respectively. Furthermore, the concentrations of the biomass burning markers  $\text{Cl}^-$  and  $\text{K}^+$  increased from 5050 to 9370  $\mu\text{g g}^{-1}$  and from 5480 to 8090  $\mu\text{g g}^{-1}$  at ARS, respectively, and from 3360 to 6650  $\mu\text{g g}^{-1}$  and from 3630 to 7500  $\mu\text{g g}^{-1}$  at UA. Positive Matrix Factorization (PMF) identified six PM<sub>2.5</sub> sources, viz., coal combustion (CC), vehicle exhaust (VE), industrial sources (ISs), biomass burning (BB), secondary inorganic aerosol (SIA), and fugitive dust (FD). FD dominated ARS during DWH and exhibited an increase at UA during AWH, and the contribution of BB at both sites rose between DWH and AWH, which can be ascribed to the burning of biomass for maize planting. Surprisingly, owing to the operation of harvesters and cultivators, the proportion of VE emissions was larger at ARS than UA. However, UA displayed a far greater percentage of industry-derived PM<sub>2.5</sub>, suggesting that local ISs should be controlled more strictly. Finally, the sizable share attributed to CC at both ARS and UA demonstrates the continued use of this fuel source, despite the governmental decree limiting it.

**Keywords:** Wheat harvest, PM<sub>2.5</sub>, Elements and ions, PMF, Beijing-Tianjin-Hebei

## 1 INTRODUCTION

North China Plain (NCP), one of two largest agricultural bases in eastern China, where the behaviors include winter wheat harvest in June and subsequent open burning of agricultural residues in field for maize planting are common. Open burning of wheat straw prevails in NCP due to low cost, convenience and insecticidal effect despite the straw burning prohibition in recent China (Wang *et al.*, 2015; Li *et al.*, 2020a, 2020b; Zhang *et al.*, 2020). Large amounts of fugitive dust release from the disturbance of dust absorbed in wheat straw and surface soil by harvesters,

## OPEN ACCESS



**Received:** February 3, 2021

**Revised:** April 3, 2021

**Accepted:** April 7, 2021

### \* Corresponding Authors:

Zhiyong Li  
lzy6566@126.com  
Xin Wang  
wx70@163.com

### Publisher:

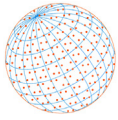
Taiwan Association for Aerosol  
Research

ISSN: 1680-8584 print

ISSN: 2071-1409 online

**Copyright:** The Author(s).

This is an open access article distributed under the terms of the [Creative Commons Attribution License \(CC BY 4.0\)](https://creativecommons.org/licenses/by/4.0/), which permits unrestricted use, distribution, and reproduction in any medium, provided the original author and source are cited.



wind, and cultivators (Li *et al.*, 2020a, 2020b). Qiu and Pattey (2008) reported that the emission rate and factor for PM<sub>10</sub> during WH period were up to  $0.58 \pm 0.12 \text{ g m}^{-2}$  and  $0.74 \pm 0.12 \text{ kg ha}^{-1}$ , respectively. Exposure to high level of agricultural dust can result in adverse health effects including acute and chronic bronchitis, mucous membrane irritation, allergic asthma and hypersensitivity, etc. (Ou *et al.*, 2020; Rao *et al.*, 2020). Also the subsequent straw burning for maize planting can result in the releasing of drastic amounts of pollutants such as CO<sub>2</sub>, CO, NH<sub>3</sub>, non-methane hydrocarbon, elemental carbon, organic carbon, and particulate matter, which influence air quality, air visibility, human health, and the climate (Chen *et al.*, 2018; Zhang *et al.*, 2020). The carbonaceous aerosols related to biomass burning contribute approximately 42% and 74% of black carbon (BC) and organic carbon (OC) globally, in which open burning of biomass accounts for 95% and 88%, respectively (Yao *et al.*, 2017). More than 50% emissions of PM<sub>2.5</sub>, OC, EC, K, K<sup>+</sup>, and Cl<sup>-</sup> in eastern China was associated with wheat straw burning (Li *et al.*, 2014).

As a large agricultural country, China contributed more than 24% of global carbonaceous aerosols, especially from field burning of biomass. The particulate matter (PM) emissions related to agricultural operations has constituted an emerging issue about air quality, especially in the areas between rural and urban environments (Qiu and Pattey, 2008; Wang *et al.*, 2015). Biomass burning has a significantly adverse effect on regional air quality, global climate change through complex feedbacks with radiation and clouds, and public health ascribed to exposure to the derived gaseous and aerosol particles (Wang *et al.*, 2015; Li *et al.*, 2020a, 2020b; Liu *et al.*, 2020).

Winter wheat mainly planted in North China Plain especially in Beijing-Tianjin-Hebei (BTH) region. The straw burning for maize plants in June after wheat harvest was common behavior because of its low cost, convenience, and insecticidal effect (Wang *et al.*, 2015; Li *et al.*, 2020b). Li *et al.* (2020a, 2020b) reported the transport mode of air pollutants as “rural to urban” for particulate matters during wheat harvest and organic pollutants after wheat harvest due to the open burning of wheat straw.

To our knowledge, the current studies mainly focused on the emission factors of PM during wheat harvest or the impact of subsequent biomass burning on local and urban areas (Qiu and Pattey, 2008; Yao *et al.*, 2017; Chen *et al.*, 2018).

## 2 METHODOLOGY

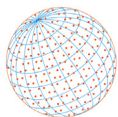
### 2.1 Description of PM<sub>2.5</sub> Sampling Sites and Campaign

The sampling locations had been shown in Li *et al.* (2021). Two collected sampling sites locate within Baoding Prefecture, which are an urban area (UA; 115°31'E, 38°53'N) in Baoding city and an adjacent rural site (ARS; 115°8'E, 38°40'N) in Wangdu County. Both UA and ARS locate in the central area of Beijing-Tianjin-Shijiazhuang triangle area. ARS within Wangdu County locates 58 km south of Baoding city. Wangdu County (115°01'–115°18'E, 38°30'–38°48'N), covers an area of 374 km<sup>2</sup> and has a permanent population of 275,000 (including 229,000 agricultural population), which is a big agricultural county with the wheat planting area of 18,095 hectares.

Two medium-volume air samplers (TH-150C) setting at 100 L min<sup>-1</sup> were used to consecutively collect PM<sub>2.5</sub> samples from June 18 to July 7 for both UA and ARS, and each sampling process lasted for 23 h. The quartz filter (QF) with 90 mm diameter was used to the analysis of 9 inorganic ions including Ca<sup>2+</sup>, K<sup>+</sup>, Mg<sup>2+</sup>, Na<sup>+</sup>, NO<sub>3</sub><sup>-</sup>, SO<sub>4</sub><sup>2-</sup>, Cl<sup>-</sup>, F<sup>-</sup>, and NH<sub>4</sub><sup>+</sup>. Teflon filter (TEF) was adopted to calculate the PM<sub>2.5</sub> mass by subtracting its pre-weight from post-weight and analyze 39 inorganic elements (IEs): Li, Be, Na, P, K, Sc, V, Cr, Mn, Co, Ni, Cu, Zn, As, Rb, Y, Mo, Cd, Sn, Sb, Cs, La, Ce, Sm, W, Tl, Pb, Bi, Th, Si, Al, Ca, Mg, Fe, Ti, Ba, Sr, and Zr. A series of field blank experiments were conducted to correct subsequent analysis deviation and ensure its accuracy. Both QFs and TEFs were purified prior to PM<sub>2.5</sub> sampling. The heating temperature was set as 450°C and 60°C for QFs and TEFs before PM<sub>2.5</sub> collections. A room with constant temperature of 20°C and relative humidity of 50% was used to store filters before and after sampling aiming to the obtainment of PM<sub>2.5</sub> mass.

### 2.2 Analysis of PM<sub>2.5</sub>-associating Inorganic Elements

The detailed detection procedure documented in Li *et al.* (2019) was adopted in this study. An inductively coupled plasma mass spectrometry (ICP-MS) system (7500A Series; Agilent, USA) was



used to detect 30 IEs including Li, Be, Na, P, K, Sc, V, Cr, Mn, Co, Ni, Cu, Zn, As, Rb, Y, Mo, Cd, Sn, Sb, Cs, La, Ce, Sm, W, Tl, Pb, Bi, Ti and Th. The rest 7 IEs involving Si, Al, Ca, Mg, Fe, Ba, and Sr were analyzed by an inductively coupled plasma atomic emission spectroscopy (ICP-OES) system (5100 Series; Agilent, USA). For ICP-MS system, the half TEF filter was heated using the both aqua regia and hydrofluoric acid at 120°C and lasted for 2 h, and then ramped to 130°C for dryness. Then it was heated again with HCl acid and stored in a plastic comparison tube for analysis. For ICP-OES, the other half TEF filter was heated at 300°C and then raised to 550°C for completely ashing. Then it was heated together with added absolute ethanol and NaOH, and boiled with water later. Finally, 2 mL HCl was added and diluted to 10 mL for analysis. This study used the standard soil materials named as GBW07446–07457 purchased from Chinese Center for National Standard Material to ensure the accuracy of ICP-MS and ICP-OES. The method detection limits fluctuated from 0.10 ng of Be to 1800 ng of Fe. The relative standard deviation (RSD) values were in the range of 2.12–6.15%.

### 2.3 Analysis of PM<sub>2.5</sub>-associating Water-soluble Ions

In regard to water-soluble ions (WSIs), half QF filter was firstly put into the centrifuge tube and underwent 20 min ultrasonic extraction with 10 mL ultra-pure deionized water for three times, and then filtered by a TEF membrane with pore size as 0.22 μm (Whatman; Middlesex, UK). Finally, the extract was transferred into a plastic bottle and stored at 4°C before analysis.

ICS-1000 system (Thermo Scientific, USA) was used to detect SO<sub>4</sub><sup>2-</sup>, NO<sub>3</sub><sup>-</sup>, Cl<sup>-</sup>, and F<sup>-</sup>, and their MDLs were in the range of 0.005–0.012 μg mL<sup>-1</sup>. K<sup>+</sup>, Na<sup>+</sup>, Ca<sup>2+</sup>, and Mg<sup>2+</sup> were analyzed using ICP-OES (725 Series; Agilent, USA) with the MDLs fluctuating from 0.002 to 0.025 μg mL<sup>-1</sup>. NH<sub>4</sub><sup>+</sup> was measured using the ultraviolet-visible (UV-Vis) spectrophotometer (T6; Beijing General Instruments Co., Ltd) and its MDL was 0.01 μg mL<sup>-1</sup>. Standard solutions corresponding to these 9 ions were obtained from the Research Center of China National Standard Reference Materials.

### 2.4 Source Apportionment of PM<sub>2.5</sub> by Positive Matrix Factorization

Positive Matrix Factorization (PMF) is a convenient multivariate factor analysis method based on non-negative constraints to get more practical factors (Yao *et al.*, 2016). PMF version 5.0 available at the U.S. EPA website (<https://www.epa.gov/air-research/positive-matrix-factorization-model-environmental-data-analyses>) was applied to evaluate PM<sub>2.5</sub> potential source contributions. The input data profiles include concentration and uncertainty values for 39 inorganic elements and 9 water-soluble ions. The abnormal concentration values were excluded to prevent error and uncertainty was calculated as Eqs. (1) and (2):

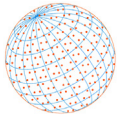
$$\text{For } c_i \leq \text{MDL, unc} = 5/6 \times \text{MDL} \quad (1)$$

$$\text{For } c_i \geq \text{MDL, unc} = [(c_i/5)^2 + \text{MDL}^2]^{0.5} \quad (2)$$

The half of MDL was utilized to represent the corresponding mass content below MDL for chemicals. The geometric mean of the observed values was used as substitutes for missing values and four times the geometric mean represented their uncertainties (Zhang *et al.*, 2015; Yao *et al.*, 2016; Zong *et al.*, 2016). A total of 20 runs were conducted for each chemical component. The lowest Q<sub>robust</sub> value was 3088.20, and the ratio of Q<sub>robust</sub>/Q<sub>true</sub> was 0.91.

A total of six emission sources including biomass burning (BB), coal combustion (CC), industrial sources (ISs), vehicle exhaust (VE), fugitive dust (FD), and secondary inorganic aerosol (SIA) were discriminated by PMF.

The BB was characterized by high loadings of Cl<sup>-</sup>, K, and K<sup>+</sup>. He *et al.* (2017) and Feng *et al.* (2018) reported that K<sup>+</sup> and NH<sub>4</sub><sup>+</sup> were commonly used markers for BB, and Cl<sup>-</sup> was also used to identify the activities of wood burning and agricultural residues. The factor with high contributions of Cu, Zn, and Pb was recognized as VE. Cu, Zn, and Pb were widely used as markers for VE (Xue *et al.*, 2019). The motor brake wears were often associated with Cu and Pb, while Zn was related to tire wears (Liu *et al.*, 2015). Pb could no longer be act as a single VE marker because of its sharply decreased concentrations owing to the prohibition of Pb containing gasoline (Li *et al.*, 2020b). Coal combustion profile is expressed by high loadings of As, Sb, and Cd, and medium



concentrations of Pb and Tl (Li *et al.*, 2016). As acting as a unique tracer of CC is frequently documented (Tao *et al.*, 2014; Li *et al.*, 2016; Yao *et al.*, 2016). Pb, Sb, and Tl often released from coal combustion despite they are typical crustal elements (Zhang *et al.*, 2014; Zong *et al.*, 2016). The factor possessing high levels of water-soluble ions including  $\text{NH}_4^+$ ,  $\text{NO}_3^-$ , and  $\text{SO}_4^{2-}$  is always associated with SIA (Yao *et al.*, 2016). Suspended dust was common in cities and rural areas due to the dust from unpaved roads, construction sites, and bare soil around urban area heaped by wind. Fugitive dust in this study features by high contents of Al, Mg, Si, Ca, Ti, Fe, and Ba. Previous studies had used Al, Mg, Si, Ca, Fe, and Ti as markers for road dust and crustal soil (Harrison *et al.*, 2012; Vossler *et al.*, 2016). In UA, the ISs are marked by high contributions of a host metal elements including K, Cr, Mn, Cu, Zn, Rb, Mo, Cd, Co, Tl, Sn, Pb, and W. The elements Mn and Cr can be considered as the steel-associating metals (Tao *et al.*, 2014; Li *et al.*, 2016), while Zn and K are often related to iron and steel processing (Li *et al.*, 2021). Cd and Co are also associated with steel processing or other metallic industrial processes (Mooibroek *et al.*, 2011). Tl, Sn, Co and Cu were frequently used in electroplating industry, and Al and Cr were mainly used in small electroplating workshops (Lestari and Mauliadi, 2009). Fe, Mn, Zn, Cd, and Ni were also used as indicators of alloy industry. Li and Pb were often associated with battery manufacturing (Yu *et al.*, 2011). A large number of electroplating and battery enterprises in Baoding further proved this inference. However, the ISs in rural area of Wangdu County differed from those of UA, which possessed lower contributions of Li and Pb due to the lack of local battery factories.

## 2.5 Geo-accumulation Indexes of Inorganic Elements (IEs)

A parameter, the geo-accumulation index ( $I_{geo}$ ), was widely used to evaluate the pollution degrees of IEs (Li *et al.*, 2017, 2019), which could be obtained by Eq. (3), where  $C_n$  are the contents of elements in  $\text{PM}_{2.5}$  and  $B_n$  are their soil background standard values in Hebei Province:

$$I_{geo} = \text{Log}_2(C_n/B_n) \quad (3)$$

The pollution levels of individual elements including uncontaminated, uncontaminated to moderately contaminated, moderately contaminated, moderately to heavily contaminated, heavily contaminated, heavily to extremely contaminated, and extremely contaminated were identified according to the  $I_{geo}$  values of  $\leq 0$ , 0–1, 1–2, 2–3, 3–4, 4–5, and  $> 5$ , respectively.

## 3 RESULT AND DISCUSSION

### 3.1 Levels of $\text{PM}_{2.5}$ , Water-soluble Ions, and Elements of UA and ARS

Fig. 1 showed the mass and volume concentrations for inorganic elements and water-soluble ions during DWH and AWH for ARS and UA.  $\text{PM}_{2.5}$  concentrations of UA fluctuated from  $23.4 \mu\text{g m}^{-3}$  of June 22 to  $200 \mu\text{g m}^{-3}$  of June 18 with a mean value as  $87.7 \mu\text{g m}^{-3}$ , and which ranged from  $23.3 \mu\text{g m}^{-3}$  of July 1 to  $155 \mu\text{g m}^{-3}$  of June 19 averaging at  $66.3 \mu\text{g m}^{-3}$ . It should be noted that higher  $\text{PM}_{2.5}$  levels appeared in ARS instead of UA indicating that the strong impact of wheat harvest activities on  $\text{PM}_{2.5}$  level (Qiu and Pattey, 2008; Zhang *et al.*, 2020; Li *et al.*, 2021). Generally,  $\text{PM}_{2.5}$  peaks appeared earlier in ARS than corresponding peaks of UA combining with air mass origin analysis of UA indicated that pollutant migration from rural to urban. Both UA and ARS possessed much higher  $\text{PM}_{2.5}$  concentrations in DWH compared with AWH, which implied that the influence of running of wheat harvesters and wheat transportation (Li *et al.*, 2020a, 2020b, 2021). The average  $\text{PM}_{2.5}$  concentrations in DWH for ARS and UA were  $156$  and  $137 \mu\text{g m}^{-3}$ , which were well above the threshold value of  $75 \mu\text{g m}^{-3}$  in the Chinese National Ambient Air Quality Standard Grade II (GB3095-2012). The  $\text{PM}_{2.5}$  levels (reported in  $\mu\text{g m}^{-3}$ ) in ARS and UA were much higher than 116 of Handan in 2014 (Meng *et al.*, 2016), 108 of Hangzhou during 2014 to 2015 (Liu *et al.*, 2015), 108 and 86.8 of Beijing in 2000–2009 and 2010–2016 (Xu *et al.*, 2017; Zhu *et al.*, 2018), 121 of Lanzhou in 2012 (Tan *et al.*, 2017), 91.7 of Shijiazhuang in 2016 (Lang *et al.*, 2018), 100.6 of Xinxiang in 2015 (Feng *et al.*, 2018), 38.9 of Ningbo in 2014–2015 (Zhang *et al.*, 2018), and 62.5 of a background site of North China Plain in 2011 (Yao *et al.*, 2016). High  $\text{PM}_{2.5}$  concentrations caused by wheat harvest behaviors should be paid more attentions under the background of present downward trend of  $\text{PM}_{2.5}$  levels on a national scale (Li *et al.*, 2020a, 2020b).

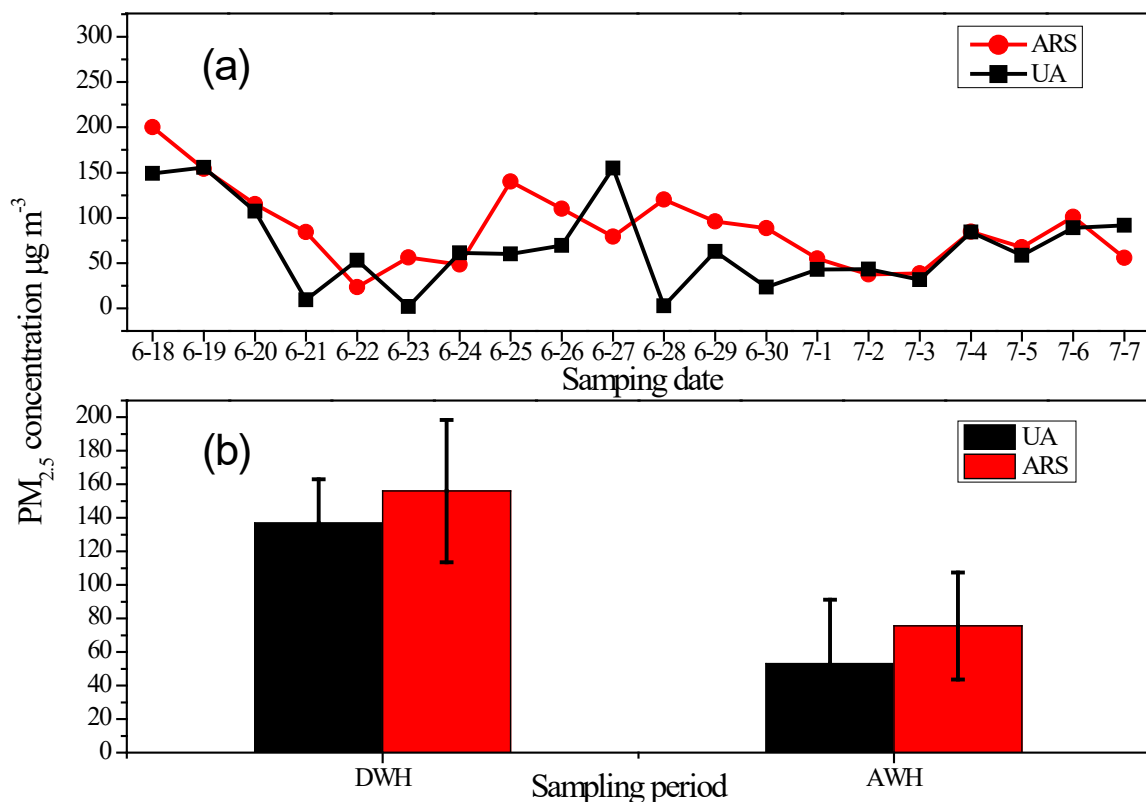
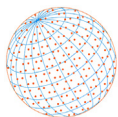


**Fig. 1.** (a) Time series of PM<sub>2.5</sub> mass concentrations and (b) average PM<sub>2.5</sub> levels during DWH and AWH for ARS and UA.

### 3.2 Time Series of Dust Levels and Trace Element Oxides

Concerning the mass contents, the sum of 39 elements and 9 ions ranged from 134 mg g<sup>-1</sup> of June 30 to 963 mg g<sup>-1</sup> of July 3 and averaged at 444 mg g<sup>-1</sup> for ARS. They varied from 224 mg g<sup>-1</sup> of July 5 to 951 mg g<sup>-1</sup> of June 23 with a mean value of 450 mg g<sup>-1</sup> for UA.

Si, Ca, Al, Fe, and Ti were major crustal elements and could be used to calculate the soil dust (SD) mass with the expression as  $[SD] = 1.89 \times [Al] + 2.14 \times [Si] + 1.4 \times [Ca] + 1.43 \times [Fe] + 1.66 \times [Mg] + 1.67 \times [Ti]$  (Su *et al.*, 2017). Among crustal elements, the elements other than Si, Al, Fe, K, Ca, Mg, Na, and Ti were defined as trace elements. Trace element oxides (TEOs) were evaluated by  $TEO = 1.3 \times [0.5 \times (Sr + Ba + Mn + Co + Rb + Ni + V) + 1.0 \times (Cu + Zn + Mo + Cd + Sn + Sb + Tl + Pb + As + Se + Ge + Cs + Ga)]$  (Zhang *et al.*, 2013). Due to the lack of Se, Ge, Cs, and Ga, the TEO was underestimated slightly.

Figs. 2 and 3 showed the time series of soil dust mass shares and TEO contents in PM<sub>2.5</sub>, and the corresponding values during DWH, AWH, and WSP. Dust shares declined significantly from 9.40% to 6.75%, and from 21.3% to 7.98% for UA and ARS with the transition from DWH to AWH. It clearly evidenced that the wheat harvest behaviors caused the re-suspending of the dust absorption in wheat straws.

The dust mass contributions ranged from 3.06% of June 18 to 12.9% of June 19 and averaging at 7.17% during whole sampling period (WSP) for UA, while higher corresponding values varied from 3.07% of June 22 to 27.1% of June 18 with a mean value as 9.99% for ARS. Higher dust mass shares attributing to ARS reflected the emissions of large amounts of dust associating with wheat harvest. UA possessed much higher dust fractions of 9.40% than the 4.6% of a background site in NCP (Yao *et al.*, 2016) and 6.4% of Chengdu in summer (Tao *et al.*, 2014), which indicated the impact of wheat harvest activities of the adjacent rural areas on air PM<sub>2.5</sub> compositions in urban areas. The average dust fraction 21.3% of ARS during DWH was also significantly higher than 13.2% of spring with frequent high concentrations of fugitive dust in a background site of NCP (Yao *et al.*, 2016), which further proved the strong influence of wheat harvest behavior.

However, TEO contents exhibited the reverse variation trends: Higher values occurred during AWH instead of DWH. The TEO contents increased from 0.079% to 0.240% for UA, and from

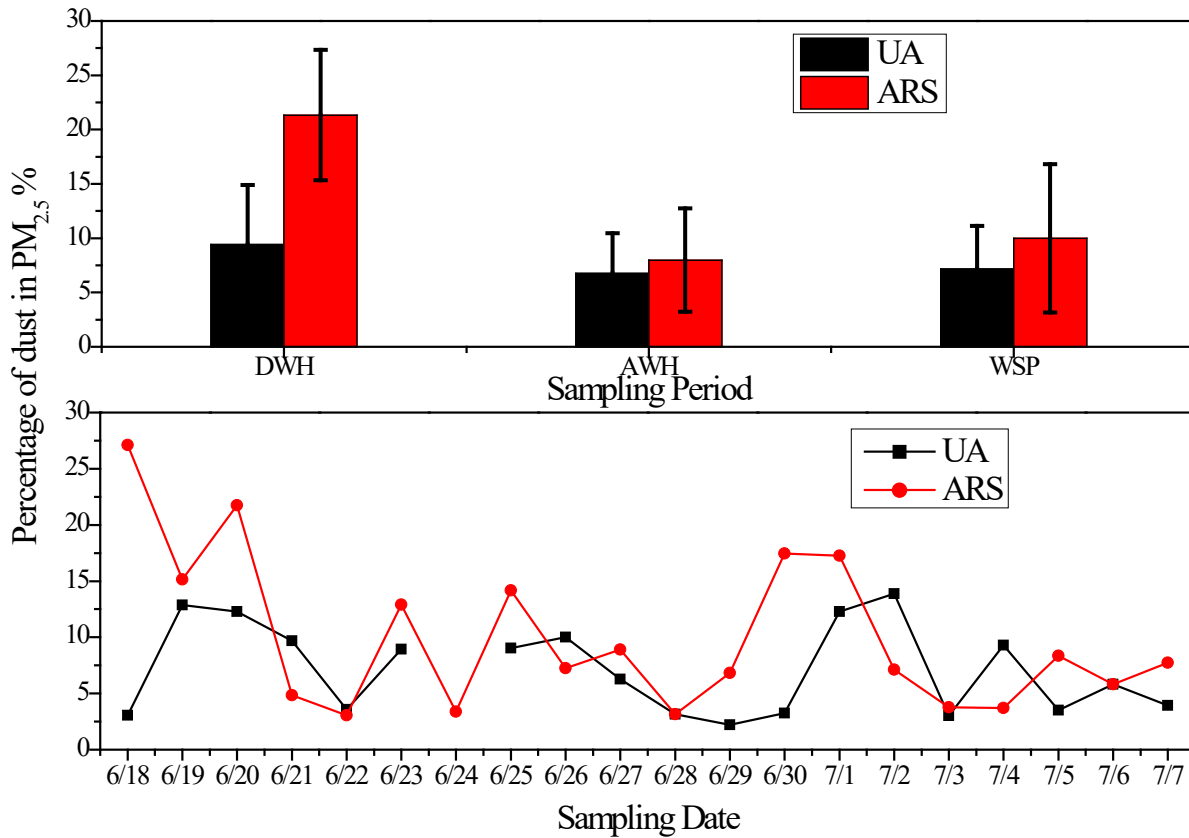
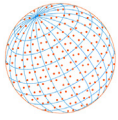


Fig. 2. Mass fractions of soil dust in  $PM_{2.5}$  during sampling period for UA and ARS.

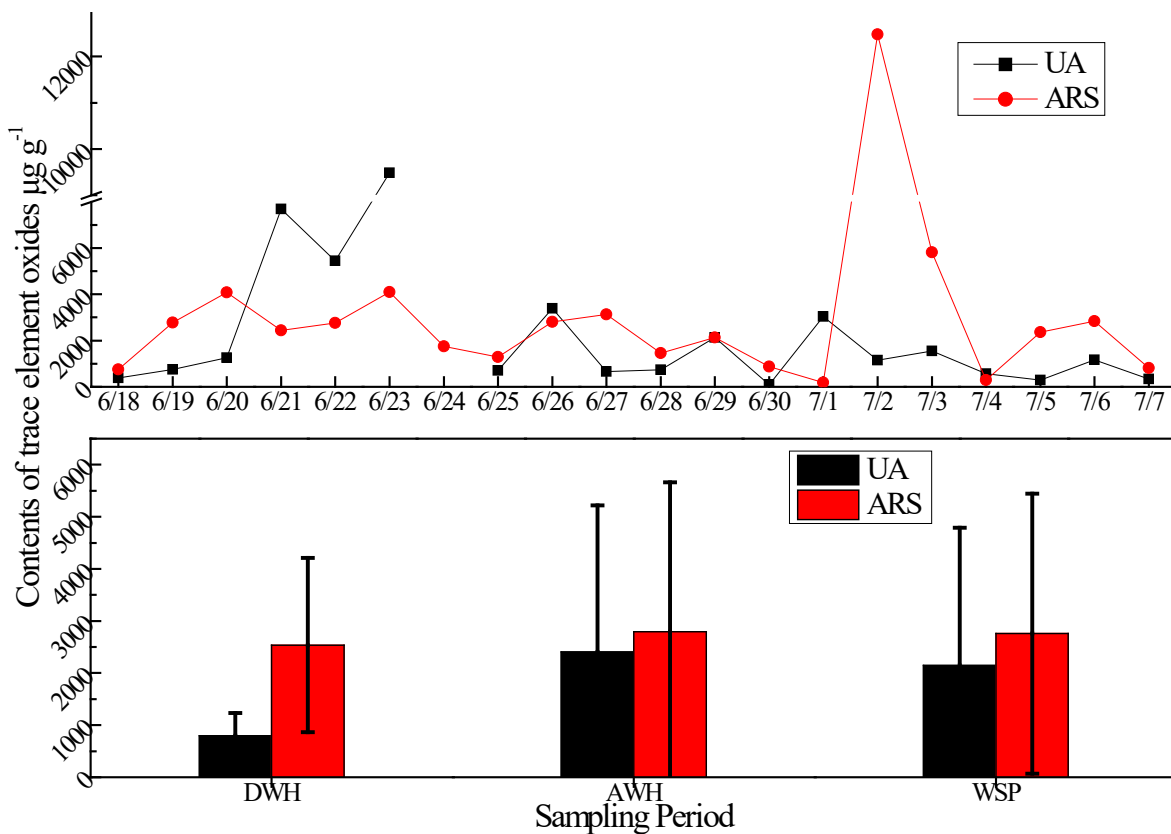
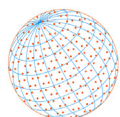


Fig. 3. Mass contents of trace element oxides during every sampling day and periods for UA and ARS.



0.254% to 0.280% along with the transition from DWH to AWH. Large amounts of trace elements emitted from wheat straw burning resulted in high TEO contents during AWH. Tao *et al.* (2014) and Zong *et al.* (2016) indicated that the biomass burning was an important source of trace elements. The TEO contents in UA and ARS were much lower than 7.2% of the adjacent Shijiazhuang in 2016, indicated the effectiveness of coal limitation and control of industrial emissions (Lang *et al.*, 2016). At the same time, higher TEO levels belonged to ARS instead of UA further verified the validity of the reduction measures adopted in industrial sources. Li *et al.* (2020a, 2020b, 2021) implied large industrial emissions of TEO from industries.

### 3.3 $I_{geo}$ Values for the Inorganic Elements

PM<sub>2.5</sub>-bounded heavy metals (HMs) and As could threaten the human health and have been widely concerned (Mario *et al.*, 2018; Li *et al.*, 2019). Table 1 showed the  $I_{geo}$  values for 39 inorganic elements for UA and ARS. The crustal elements such as Al, Mg, Ca, Fe, and Ti for both UA and ARS possessed high  $I_{geo}$  values, which varied from 3.31 to 6.26 for ARS, and from 1.62 to 5.38 for UA (Table 1). Higher  $I_{geo}$  values of crustal elements in ARS reflected the impact of WH-related activities. Also higher Cu and Zn  $I_{geo}$  values in ARS suggested the influence of running of agricultural machineries. Considering HMs, Cd, Sb, Sn, Mo, and Pb possessed high  $I_{geo}$  values reflecting the impact of industrial production processes and coal combustion.

### 3.4 Levels of the Water-soluble Ions

The sum of mass contents of 9 WSIs were in the range of 0.051 g g<sup>-1</sup> of June 30 to g g<sup>-1</sup> of June 21 averaging at 0.321 g g<sup>-1</sup> for UA. The corresponding values for ARS varied from 0.095 g g<sup>-1</sup> of June 30 to 0.871 g g<sup>-1</sup> of July 3 with a mean value as 0.394 g g<sup>-1</sup>. SO<sub>4</sub><sup>2-</sup>, NO<sub>3</sub><sup>-</sup>, and NH<sub>4</sub><sup>+</sup> (SNN) dominated in 9 WSIs for both UA and ARS; SNN contributed 92.0% and 90.3% to total mass of 9 WSIs for UA and ARS, respectively. No significant differences concerning the mass contents of SO<sub>4</sub><sup>2-</sup>, NO<sub>3</sub><sup>-</sup>, and NH<sub>4</sub><sup>+</sup> existed between DWH and AWH for both UA and ARS, which reflected the emissions sources of them were similar between these two periods (Fig. S1). The mass ratios of NO<sub>3</sub><sup>-</sup>/SO<sub>4</sub><sup>2-</sup> during DWH and AWH were 0.993 and 0.832 for ARS, and 1.21 and 0.718 for UA, which indicated that coal combustion except for DWH of UA was still an important source despite the coal limitation policy in China (Zhai *et al.*, 2019).

Acting as the markers of biomass burning, Cl<sup>-</sup> and K<sup>+</sup> increased along with the transition from DWH to AWH for both UA and ARS (Fig. 4). ARS possessed higher contents of these two ions than UA indicating the strong influence of local biomass burning during AWH in rural area. Concerning UA, Cl<sup>-</sup> contents fluctuated from 3080 to 3510 μg g<sup>-1</sup> during DWH, and from 1390 to 29,100 μg g<sup>-1</sup> during AWH. For ARS, they ranged from 3870 to 6300 μg g<sup>-1</sup> for ARS during DWH, and from 1710 to 18,000 μg g<sup>-1</sup> during AWH. K<sup>+</sup> contents varied from 2960 to 4210 μg g<sup>-1</sup> and 2040 to 35,900 μg g<sup>-1</sup> during DWH and AWH for UA, and from 3930 to 8050 μg g<sup>-1</sup> and 2310 to 21,600 μg g<sup>-1</sup> for

**Table 1.**  $I_{geo}$  values of elements for ARS and UA.

Element	$I_{geo}$		Element	$I_{geo}$		Element	$I_{geo}$	
	ARS	UA		ARS	UA		ARS	UA
Li	-3.27	-3.79	Rb	-4.51	-4.86	Bi	3.44	2.68
Be	-4.57	-5.29	Y	-4.64	-5.4	Th	-5.04	-5.86
Na	5.51	3.37	Mo	1.55	1.35	U	-4.26	-4.8
K	5.17	2.56	Cd	5.19	4.81	Zr	-4.2	-3.94
Sc	-4.18	-4.09	Sn	1.36	1.77	Al	3.31	1.62
V	-3.89	-4.22	Sb	2.38	2.34	Sr	-2.86	-3.26
Cr	-2.31	-2.15	Cs	-3.46	-3.76	Mg	6.26	4.31
Mn	-2.96	-3.36	La	-4.62	-5.23	Ti	7.53	5.38
Co	-3.52	-4.1	Ce	-4.73	-5.33	Ca	4.93	3.17
Ni	-1.83	-0.41	Sm	-4.82	-5.78	Fe	4.56	2.64
Cu	4.61	0.88	W	3.46	-0.32	Ba	-2.45	-3.54
Zn	3.07	2.22	Tl	1.42	1.34			
As	0.16	-0.04	Pb	1.95	1.68			

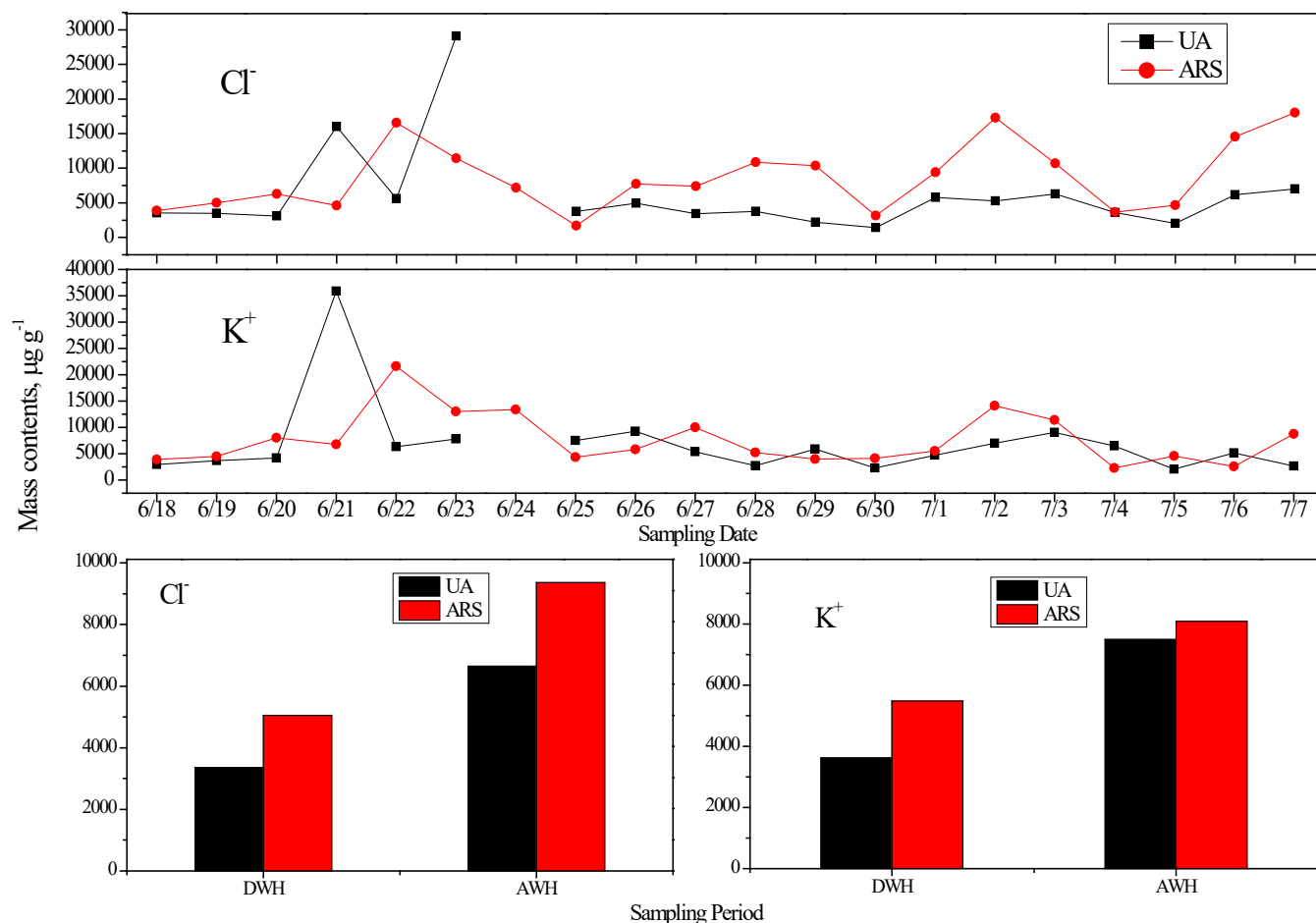
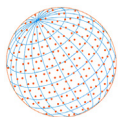


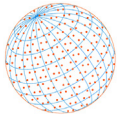
Fig. 4. Contents of Cl<sup>-</sup> and K<sup>+</sup> during each sampling day and period for UA and ARS.

ARS. However, the mass concentrations (reported in µg m<sup>-3</sup>) of Cl<sup>-</sup> and K<sup>+</sup> showed the reverse trends: Higher values occurred during DWH for both UA and ARS attributing to high PM<sub>2.5</sub> mass concentrations during DWH. Cl<sup>-</sup> and K<sup>+</sup> mass concentrations for UA during DWH were 0.466 and 0.490 µg m<sup>-3</sup>, which were almost two times 0.241 and 0.274 µg m<sup>-3</sup> for AWH. Higher corresponding values of Cl<sup>-</sup> and K<sup>+</sup> appeared in ARS, which were 0.755/0.800 and 0.629/0.493 µg m<sup>-3</sup> during DWH and AWH, respectively. The mass concentrations of Cl<sup>-</sup> and K<sup>+</sup> (reported in µg m<sup>-3</sup>) for both UA and ARS were much lower than 3.69 and 1.18 for Shijiazhuang in autumn of 2016 (Lang *et al.*, 2018), and 2.0 and 2.3 for Beijing in summer of 2012 (Zhang *et al.*, 2016). Lower Cl<sup>-</sup> and K<sup>+</sup> contents than some cities implied the effectiveness of emission control of related sources such as biomass burning and coal combustion (Li *et al.*, 2020a, 2020b, 2021; Zhai *et al.*, 2019).

SNN mass concentrations also exhibited the same trends with Cl<sup>-</sup> and K<sup>+</sup>: DWH possessed higher values due to its higher PM<sub>2.5</sub> levels compared than AWH. DWH possessed higher SO<sub>4</sub><sup>2-</sup>, NO<sub>3</sub><sup>-</sup>, and NH<sub>4</sub><sup>+</sup> mass concentrations (reported in µg m<sup>-3</sup>) 21.7, 21.6, and 14.6 for ARS, and 15.0, 18.2 and 11.8 for UA. Lower corresponding values during AWH 9.11, 7.58, and 6.51, and 6.19, 4.44, and 4.32 appeared in ARS and UA, respectively. The SNN concentrations in UA and ARS were lower than 28.4, 34.6, and 13.1 of Beijing in summer of 2012 (Zhang *et al.*, 2016).

### 3.5 Source Apportionment by PMF for UA and ARS

Fig. 5 showed the source fractions during DWH, AWH, and WSP. It should be noted that BB shares in ARS increased from 5.27% to 25.5% along with the DWH to AWH, and the corresponding shares enhanced from 1.68% to 14.4% for UA. The similar increasing trends between UA and ARS, and higher BB shares in ARS proved the impact of open biomass burning for maize planting after wheat harvest in rural areas (Li *et al.*, 2020a, 2020b, 2021). Higher contribution of FD was attributed to ARS, which was 22.81% during whole sampling period. Under the wheat harvest activities, the



Biomass burning Fugitive dust Secondary inorganic aerosols Vehicle emissions  
Coal combustion Industrial sources

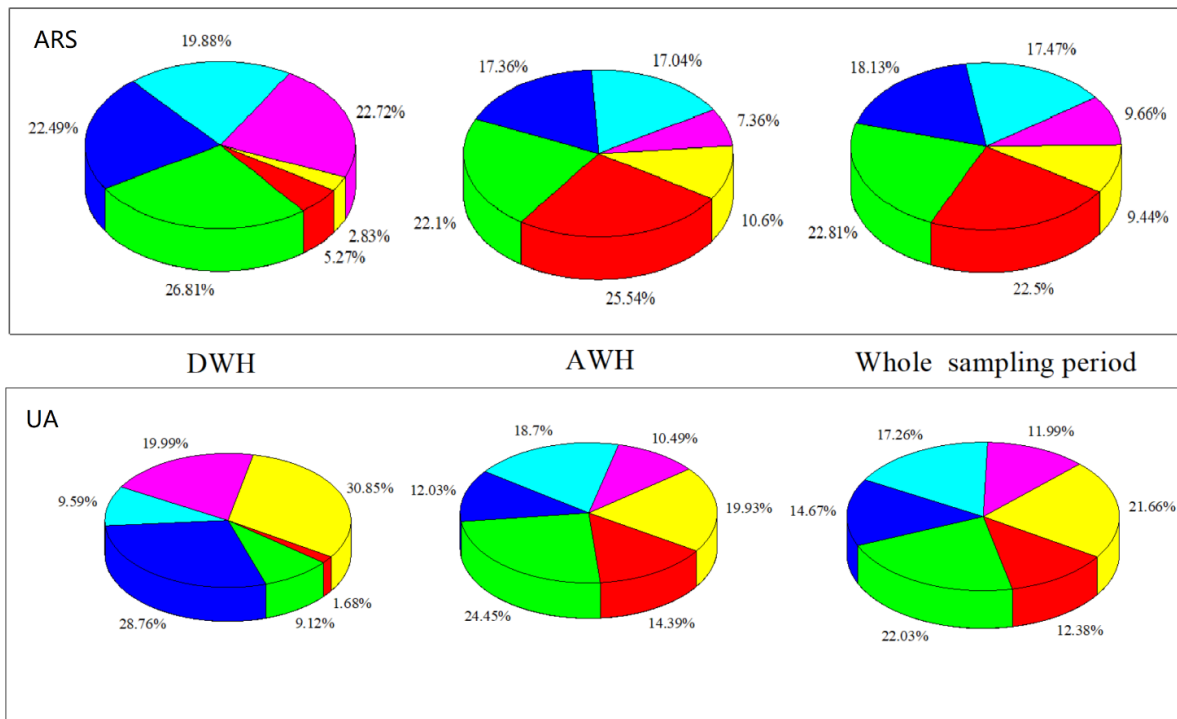


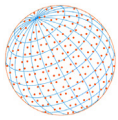
Fig. 5. The contributions of six sources to the  $PM_{2.5}$  for ARS and UA.

adjacent UA also possessed considerable FD contribution of 22.0% during WSP. Higher FD share 26.8% occurred during DWH for ARS, while it was 24.5% during AWH for UA. More direct influence in rural area from WH-related activities such as running of wheat harvesters and wheat transportation was the explanation of higher FD shares during DWH for ARS. The surprised higher FD during AWH share 24.5% occurred in UA instead of ARS (22.1%) suggesting that urban areas possessed some unique FD sources such as extensive construction of buildings and road dust. At the same time, due to the highly intensive operation of large amounts of wheat harvesters and wheat transportation tractors, ARS possessed higher VE contributions than UA during DWH. However, VE shares during AWH in UA were higher than ARS, which might be associated with the decrease of operation intensity of harvesters. It was important to note that VE still occupying a high share during AWH for ARS, which might be related to the running of rotary cultivators for maize planting and vehicles for fertilizer transportation. Much higher IS contribution 30.9% occurred in UA during DWH and subsequently decreased to 19.9% due to the increasing shares of BB and FD. High IS shares should be concerned by local government, and strict emission standards and appropriate control measures were urgent to developed. The secondary inorganic aerosol was a key contributor for UA and ARS during both DWH and AWH. CC contributed 12.0% and 9.66% to the total  $PM_{2.5}$  mass for UA and ARS indicating coal was still an important fuel used in events including urban industrial production and rural cooking (Li *et al.*, 2020a, 2020b, 2021).

The contributions of FD and BB in UA and ARS associating with wheat harvest were much higher than Shijiazhuang, background site of North China Plain, Chengdu, Nanjing, and Lanzhou (Table S1). The VE possessed higher shares in UA and ARS than abovementioned cities due to the operation of wheat harvesters and rotary cultivators.

## 4 CONCLUSIONS

To evaluate the effects of wheat harvesting in rural regions on the air quality in adjacent urban areas, we conducted a systematic  $PM_{2.5}$  sampling campaign at both a rural and an urban site (ARS



and UA, respectively) in the center of the Beijing-Tianjin-Hebei megalopolis during and after the harvest. We then analyzed the samples to evaluate 1) the PM<sub>2.5</sub> concentrations; 2) the chemical components, specifically, 39 IEs and 9 WSIs; and 3) the differences between the two sites in terms of source contributions.

- 1) We observed higher PM<sub>2.5</sub> concentrations at ARS than UA, but both sites showed elevated levels during DWH (156 and 137  $\mu\text{g m}^{-3}$  at ARS and UA, respectively) compared to AWH (75.6 and 53.1  $\mu\text{g m}^{-3}$ , respectively). In addition, the PM<sub>2.5</sub> peaks appeared later at UA than ARS, demonstrating the rural-to-urban migration of pollution. Both locations also displayed higher  $I_{\text{geo}}$  values for the crustal elements than the other elements, confirming that the dust emissions originated from the wheat harvest.
- 2) Based on the IE content, dust composed 21.3% and 9.40% of the PM<sub>2.5</sub> mass at ARS and UA during DWH, respectively, but only 7.98% and 6.75% during AWH, further confirming the migration effect. By contrast, the mass ratios of the TEOs to the PM<sub>2.5</sub> increased from 0.254% to 0.280% and from 0.079% to 0.240% at ARS and UA, respectively, between DWH and AWH, because of straw burning emissions following the harvest.
- 3) The levels of the biomass markers  $\text{Cl}^-$  and  $\text{K}^+$  rose significantly from DWH to AWH at both sites, which is attributable to the open burning of straw for maize planting. Specifically, the  $\text{Cl}^-$  concentration varied 3870–6300  $\mu\text{g g}^{-1}$  at ARS and 3080–3510  $\mu\text{g g}^{-1}$  at UA during DWH but 1710–18,000  $\mu\text{g g}^{-1}$  and 1390–29,100  $\mu\text{g g}^{-1}$  during AWH, and the  $\text{K}^+$  concentration varied 3930–8050  $\mu\text{g g}^{-1}$  at ARS and 2960–4210  $\mu\text{g g}^{-1}$  at UA during DWH but 2310–21,600  $\mu\text{g g}^{-1}$  and 2040–35,900  $\mu\text{g g}^{-1}$  during AWH.
- 4) PMF revealed that the contribution of BB grew from 5.27% to 25.5% and from 1.68% to 14.4% at ARS and UA, respectively, between DWH and AWH. Furthermore, the share from FD peaked during DWH at ARS (26.81%) but during AWH at UA, mainly owing to the rural-to-urban transport time. Unexpectedly, the operation of agricultural machinery led to a higher proportion of VE emissions at ARS than UA. Lastly, CC accounted for 9.66% and 12.0% of the total PM<sub>2.5</sub> mass at ARS and UA over the entire sampling period, respectively, proving that coal remains a common fuel for rural household cooking and urban industrial production.

## ACKNOWLEDGEMENTS

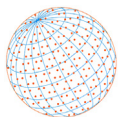
This study was supported by the Beijing Natural Science Foundation (8212034), the Natural Science Foundation of Hebei Province (B2020502007), and the Fundamental Research Funds for the Central Universities (2020MS125).

## SUPPLEMENTARY MATERIAL

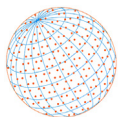
Supplementary data associated with this article can be found in the online version at <https://doi.org/10.4209/aaqr.210026>

## REFERENCES

- Chen, H.Y., Yin, S.S., Li, X., Wang, J., Zhang, R.Q. (2018). Analyses of biomass burning contribution to aerosol in Zhengzhou during wheat harvest season in 2015. *Atmos. Res.* 207, 62–73. <https://doi.org/10.1016/j.atmosres.2018.02.025>
- Feng, J.L., Yu, H., Mi, K., Su, X.F., Li, Y., Li, Q.L., Sun, J.H. (2018). One year study of PM<sub>2.5</sub> in Xinxiang city, North China: Seasonal characteristics, climate impact and source. *Ecotoxicol. Environ. Saf.* 154, 75–83. <https://doi.org/10.1016/j.ecoenv.2018.01.048>
- Harrison, R.M., Jones, A.M., Gietl, J., Yin, J.X., Green, D.C. (2012). Estimation of the contributions of brake dust, tire wear, and resuspension to nonexhaust traffic particles derived from atmospheric measurements. *Environ. Sci. Technol.* 46, 6523–6529. <https://doi.org/10.1021/es300894r>
- He, Q.S., Yan, Y.L., Guo, L.L., Zhang, Y.L., Zhang, G.X., Wang, X.M. (2017). Characterization and source analysis of water-soluble inorganic ionic species in PM<sub>2.5</sub> in Taiyuan city, China. *Atmos. Res.* 184, 48–55. <https://doi.org/10.1016/j.atmosres.2016.10.008>



- Lang, J.L., Li, S.Y., Cheng, S.Y., Zhou, Y., Chen, D.S., Zhang, Y.Y., Zhang, H.Y., Wang, H.Y. (2018). Chemical characteristics and sources of submicron particles in a city with heavy pollution in China. *Atmosphere* 9, 388–407. <https://doi.org/10.3390/atmos9100388>
- Lestari, P., Mauliadi, Y.D. (2009). Source apportionment of particulate matter at urban mixed site in Indonesia using PMF. *Atmos. Environ.* 43, 1760–1770. <https://doi.org/10.1016/j.atmosenv.2008.12.044>
- Li, H.Y., Guo, L.L., Cao, R.F., Gao, B., Yan, Y.L., He, Q.S. (2016). A wintertime study of PM<sub>2.5</sub>-bound polycyclic aromatic hydrocarbons in Taiyuan during 2009–2013: Assessment of pollution control strategy in a typical basin region. *Atmos. Environ.* 140, 404–414. <https://doi.org/10.1016/j.atmosenv.2016.06.013>
- Li, J.F., Song, Y., Mao, Y., Mao, Z.C., Wu, Y.S., Li, M.M., Huang, X., He, Q.C., Hu, M. (2014). Chemical characteristics and source apportionment of PM<sub>2.5</sub> during the harvest season in eastern China's agricultural regions. *Atmos. Environ.* 92, 442–448. <https://doi.org/10.1016/j.atmosenv.2014.04.058>
- Li, Z.Y., Wang, Y.T., Guo, S.T., Li, Z.X., Xing, Y.R., Liu, G.Q., Fang, R., Hu, Y., Zhu, H.T., Yan, Y.L. (2019). PM<sub>2.5</sub> associated PAHs and inorganic elements from combustions of biomass, cable wrapping, domestic waste, and garbage for power generation. *Aerosol Air Qual. Res.* 19, 2502–2517. <https://doi.org/10.4209/aaqr.2019.10.0495>
- Li, Z.Y., Guo, S.T., Li, Z.X., Wang, Y.T., Hu, Y., Xing, Y.R., Liu, G.Q., Fang, R., Zhu, H.T. (2020a). PM<sub>2.5</sub> associated phenols, phthalates, and water soluble ions from five stationary combustion sources. *Aerosol Air Qual. Res.* 20, 61–71. <https://doi.org/10.4209/aaqr.2019.11.0602>
- Li, Z.Y., Wang, Y.T., Li, Z.X., Guo, S.T., Hu, Y. (2020b). Levels and Sources of PM<sub>2.5</sub>-associated PAHs during and after the Wheat Harvest in a Central Rural Area of the Beijing–Tianjin–Hebei (BTH) Region. *Aerosol Air Qual. Res.* 20, 1070–1082. <https://doi.org/10.4209/aaqr.2020.03.0083>
- Li, Z.Y., Li, Z.X., Yue, Z.Y., Yang, D.Y., Wang, Y.T., Chen, L., Guo, S.T., Yao, J.S., Wang, L., Lou, X., Xu, X.L., Wei, J.Y., Deng, B.L., Wu, H. (2021). Impact of wheat harvest on levels and sources of PM<sub>2.5</sub>-associated PAHs in an urban area located at the center of Beijing–Tianjin–Hebei region. *Aerosol Air Qual. Res.* 21, 200625. <https://doi.org/10.4209/aaqr.200625>
- Liu, G., Li, J.H., Wu, D., Xu, H. (2015). Chemical composition and source apportionment of ambient PM<sub>2.5</sub> in Hangzhou, China. *Particuology* 18, 135–143. <https://doi.org/10.1016/j.partic.2014.03.011>
- Liu, L.X., Cheng, Y.F., Wang, S.W., Wei, C., Pöhlker, M.L., Pöhlker, C., Artaxo, P., Shrivastava, M., Andreae, M.O., Pöschl, U., Su, H. (2020). Impact of biomass burning aerosols on radiation, clouds, and precipitation over the Amazon: Relative importance of aerosol-cloud and aerosol-radiation interactions. *Atmos. Chem. Phys.* 20, 13283–13301. <https://doi.org/10.5194/acp-20-13283-2020>
- Mario, A., Mihaela, M., Massimo, D.I., Maurizio, G. (2018). Impact of emissions, meteorology and grid resolution on changes in HMs and PAHs concentrations between 2005 and 2010 in Italy. *Aerosol Air Qual. Res.* 18, 3165–3176. <https://doi.org/10.4209/aaqr.2017.08.0262>
- Meng, C.C., Wang, L.T., Zhang, F.F., Wei, Z., Ma, S.M., Ma, X., Yang, J. (2016). Characteristics of concentrations and water-soluble inorganic ions in PM<sub>2.5</sub> in Handan City, Hebei province, China. *Atmos. Res.* 171, 133–146. <https://doi.org/10.1016/j.atmosres.2015.12.013>
- Mooibroek, D., Schaap, M., Weijers, E.P., Hoogerbrugge, R. (2011). Source apportionment and spatial variability of PM<sub>2.5</sub> using measurements at five sites in the Netherlands. *Atmos. Environ.* 45, 4180–4191. <https://doi.org/10.1016/j.atmosenv.2011.05.017>
- Ou, C.Y., Hang, J., Deng, Q.H. (2020). Particle deposition in human lung airways: Effects of airflow, particle size, and mechanisms. *Aerosol Air Qual. Res.* 20, 2846–2858. <https://doi.org/10.4209/aaqr.2020.02.0067>
- Qiu, G.W., Pattey, E. (2008). Estimating PM<sub>10</sub> emissions from spring wheat harvest using an atmospheric trace technique. *Atmos. Environ.* 42, 8315–8321. <https://doi.org/10.1016/j.atmosenv.2008.07.022>
- Rao, Y., Li, H.Y., Chen, M.X., Fu, Q.Y., Zhuang, G.S., Huang, K. (2020). Characterization of airborne microbial aerosols during a long-range transported dust event in Eastern China: Bacterial community, influencing factors, and potential health effects. *Aerosol Air Qual. Res.* 20, 2834–2845. <https://doi.org/10.4209/aaqr.2020.01.0030>
- Su, X.L., Wang, Q., Li, Z.Q., Calvello, M., Esposito, F., Pavese, G., Lin, M.J., Cao, J.J., Zhou, C.Y., Li, D.H., Xu, H. (2017). Regional transport of anthropogenic pollution and dust aerosols in spring



- to Tianjin – A coastal megacity in China. *Sci. Total Environ.* 584–585, 381–392. <https://doi.org/10.1016/j.scitotenv.2017.01.016>
- Tan, J.H., Zhang, L.M., Zhou, X.M., Duan, J.C., Li, Y., Hu, J.N., He, K.B. (2017). Chemical characteristics and source apportionment of PM<sub>2.5</sub> in Lanzhou, China. *Sci. Total Environ.* 601–602, 1743–1752. <https://doi.org/10.1016/j.scitotenv.2017.06.050>
- Tao, J., Gao, J., Zhang, L., Zhang, R., Che, H., Zhang, Z., Lin, Z., Jing, L., Cao, J., Hsu, S.C. (2014). PM<sub>2.5</sub> pollution in a megacity of southwest China: Source apportionment and implication. *Atmos. Chem. Phys.* 14, 8679–8699. <https://doi.org/10.5194/acp-14-8679-2014>
- Vossler, T., Černíkovský, L., Novák, J., Williams, R. (2016). Source apportionment with uncertainty estimates of fine particulate matter in Ostrava, Czech Republic using Positive Matrix Factorization. *Atmos. Pollut. Res.* 7, 503–512. <https://doi.org/10.1016/j.apr.2015.12.004>
- Wang, L.L., Xin, J.Y., Li, X.R., Wang, Y.S. (2015). The variability of biomass burning and its influence on regional aerosol properties during the wheat harvest season in North China. *Atmos. Res.* 157, 153–163. <https://doi.org/10.1016/j.atmosres.2015.01.009>
- Xu, L.L., Duan, F.K., He, K.B., Ma, Y.L., Zhu, L.D., Zheng, Y.X., Huang, T., Kimoto, T., Ma, T., Li, H., Ye, S.Q., Yang, S., Sun, Z.L., Xu, B.Y. (2017). Characteristics of the secondary water-soluble ions in a typical autumn haze in Beijing. *Environ. Pollut.* 227, 296–305. <https://doi.org/10.1016/j.envpol.2017.04.076>
- Xue, H.Q., Liu, G.J., Zhang, H., Hu, R.Y., Wang, X. (2019). Similarities and differences in PM<sub>10</sub> and PM<sub>2.5</sub> concentrations, chemical compositions and sources in Hefei City, China. *Chemosphere* 220, 760–765. <https://doi.org/10.1016/j.chemosphere.2018.12.123>
- Yao, H., Song, Y., Liu, M.X., Archer-Nicholls, S., Lowe, D., McFiggans, G., Xu, T.T., Du, P., Li, J.F., Wu, Y.S., Hu, M., Zhao, C., Zhu, T. (2017). Direct radiative effect of carbonaceous aerosols from crop residue burning during the summer harvest season in East China. *Atmos. Chem. Phys.* 17, 5205–5219. <https://doi.org/10.5194/acp-17-5205-2017>
- Yao, L., Yang, L.X., Yuan, Q., Yan, C., Dong, C., Meng, C.P., Sui, X., Yang, F., Lu, Y.L., Wang, W.X. (2016). Sources apportionment of PM<sub>2.5</sub> in a background site in the North China Plain. *Sci. Total Environ.* 541, 590–598. <https://doi.org/10.1016/j.scitotenv.2015.09.123>
- Yu, Y., Schleicher, N., Norra, S., Fricker, M., Dietze, V., Kaminski, U., Cen, K., Stuben, D. (2011). Dynamics and origin of PM<sub>2.5</sub> during a three-year sampling period in Beijing, China. *J. Environ. Monit.* 13, 334–346. <https://doi.org/10.1039/c0em00467g>
- Zhai, S.X., Jacob, D.J., Wang, X., Shen, L., Li, K., Zhang, Y.Z., Gui, K., Zhao, T.L., Liao, H. (2019). Fine particulate matter (PM<sub>2.5</sub>) trends in China, 2013–2018: Separating contributions from anthropogenic emissions and meteorology. *Atmos. Chem. Phys.* 19, 11031–11041. <https://doi.org/10.5194/acp-19-11031-2019>
- Zhang, F.W., Xu, L.L., Chen, J.S., Chen, X.Q., Niu, Z.C., Lei, T., Li, C.M., Zhao, J.P. (2013). Chemical characteristics of PM<sub>2.5</sub> during haze episodes in the urban of Fuzhou, China. *Particuology* 11, 264–272. <https://doi.org/10.1016/j.partic.2012.07.001>
- Zhang, T.R., Jong, M.C.D., Wooster, M.J., Xu, W.D., Wang, L.L. (2020). Trends in eastern China agricultural fire emissions derived from a combustion of geostationary (Himawari) and polar (VIIRS) orbiter fire radiative power products. *Atmos. Chem. Phys.* 20, 10687–10705. <https://doi.org/10.5194/acp-20-10687-2020>
- Zhang, Y., Huang, W., Cai, T.Q., Fang, D.Q., Wang, Y.Q., Song, J., Hu, M., Zhang, Y.X. (2016). Concentrations and chemical compositions of fine particles (PM<sub>2.5</sub>) during haze and non-haze days in Beijing. *Atmos. Res.* 174–175, 62–69. <https://doi.org/10.1016/j.atmosres.2016.02.003>
- Zhang, Y.Y., Lang, J.L., Cheng, S.Y., Li, S.Y., Zhou, Y., Chen, D.S., Zhang, H.Y., Wang, H.Y. (2018). Chemical composition and sources of PM<sub>1</sub> and PM<sub>2.5</sub> in Beijing in autumn. *Sci. Total Environ.* 630, 72–82. <https://doi.org/10.1016/j.scitotenv.2018.02.151>
- Zhu, Y., Huang, L., Li, J., Ying, Q., Zhang, H., Liu, X., Liao, H., Li, N., Liu, Z., Mao, Y., Fang, H., Hu, J. (2018). Sources of particulate matter in China: Insights from source apportionment studies published in 1987–2017. *Environ. Int.* 115, 343–357. <https://doi.org/10.1016/j.envint.2018.03.037>
- Zong, Z., Wang, X.P., Tian, C.G., Chen, Y.J., Qu, L., Ji, L., Zhi, G.R., Li, J., Zhang, G. (2016). Source apportionment of PM<sub>2.5</sub> at a regional background site in North China using PMF linked with radiocarbon analysis: Insight into the contribution of biomass burning. *Atmos. Chem. Phys.* 16, 11249–11265. <https://doi.org/10.5194/acp-16-11249-2016>